Baird, A. F., Stork, A. L., Horne, S. A., Naldrett, G., Kendall, J-M., Wookey, J., Verdon, J. P., & Clarke, A. (2020). Characteristics of microseismic data recorded by distributed acousticsensing systems in anisotropic media. *Geophysics*, *85*(4), KS139-KS147. https://doi.org/10.1190/geo2019-0776.1

Characteristics of microseismic data recorded by Distributed Acoustic Sensing (DAS) systems in anisotropic media

A.F. Baird[*], A.L. Stork[*†], S.A. Horne[‡], G. Naldrett[†], J-M. Kendall[*§], J. Wookey[*], J.P. Verdon[*] and A. Clarke[†]

[*] *School of Earth Sciences, University of Bristol, Bristol, UK*

[†] *Silixa Ltd., London, UK*

[‡] *Formerly: Chevron Energy Technology Company, London, UK*

[§] *Department of Earth Sciences, University of Oxford, Oxford, UK*

(March 27, 2020)

Running head: **Microseismic DAS in anisotropic media**

ABSTRACT

Fiber-optic Distributed Acoustic Sensing (DAS) cables are now used to monitor microseismicity during hydraulic fracture stimulations of unconventional gas reservoirs. Unlike geophone arrays, DAS systems are sensitive to uniaxial strain or strain-rate along the fiber direction and thus provide a single-component recording, which makes identifying the directionality and polarisation of incoming waves difficult. Using synthetic examples, we show some fundamental characteristics of microseismic recordings on DAS systems for purposes of hydraulic fracture monitoring in a horizontal well in anisotropic (vertical transverse isotropy, VTI) shales. We demonstrate that SH arrivals dominate the recorded signals since their polarization is aligned along the horizontal cable at near offset, though SV will typically dominate for events directly above or below the array. The amplitude of coherent S-wave arrivals along the cable exhibits a characteristic pattern with bimodal peaks, the width of

which relates to the distance of the event from the cable. Furthermore, we find that shear-wave splitting recorded on DAS systems can be used to infer the inclination of the incoming waves, overcoming a current limitation of event locations which have constrained events to lie in a horizontal plane. Low amplitude SV arrivals suggest an event depth similar to that of the DAS cable. Conversely, steep arrivals produce higher amplitude SV waves, with shear-wave splitting increasing with offset along the cable. Finally we show how polarity reversals observed in the P and SH phases can be used to provide strong constraints on the source mechanisms.

INTRODUCTION

In the last decade, fiber-optic technology has developed to use distributed acoustic sensing (DAS) cables to measure the dynamic strain or strain-rate induced by seismic waves (Parker et al., 2014). The technology has been increasingly used to acquire downhole seismic data, predominately for vertical seismic profiling (VSP), but more recently also for monitoring of hydraulic fracture stimulation (Karrenbach et al., 2019).

The technology makes use of Rayleigh scattering of light along the fiber optic cable. An interrogator unit is used to send laser pulses into a fiber and detect the back-scattered response due to interaction with inhomogeneities along the fiber. If the fiber undergoes a localized strain, caused, for example, by a passing seismic wave, this lengthens (or shortens) the fiber causing a phase shift in the back-scattered response. These changes in phase are used to compute strain or strain-rate at a series of regularly spaced channels (or receivers) along the cable. The strain that is computed is not a point measurement, but the average value over a 'gauge' length along the cable centred at each channel.

DAS technology has a number of advantages over traditional geophone recordings. For example, a cable can be several kilometers long with the strain field sampled at closely spaced channels (on the order of meters), resulting in thousands of receivers and a very dense wavefield sampling at a relatively low cost per sensor. Conversely, downhole geophone arrays typically consist of 10s to 100s of receivers at a much wider spacing. Additionally fiber optic cables can be deployed behind casing allowing the well to be used for other purposes during monitoring, and allowing the ability to easily record and repeat surveys over months to years.

The technology also presents a number of challenges that must be overcome for use

in microseismic monitoring. For example, the large volumes of data produced by DAS systems may require the development of novel approaches, such as machine learning algorithms, to quickly process and detect events in real time (e.g. Horne et al., 2019; Binder and Chakraborty, 2019). Additionally, unlike conventional seismic sensors that measure particle motion, DAS systems are sensitive to the uniaxial strain or strain-rate along the direction of the fiber optic cable. As a result, the systems provide a single-component recording, polarized in the cable direction rather than the standard three components provided by geophones. Such differences lead to an ambiguity in the directionality of incoming waves, and some of the patterns observed in strain may run counter to intuition for those more familiar with geophone recordings of particle motion.

Here we investigate some fundamental characteristics of microseismic data recorded on DAS systems for the purposes of hydraulic fracture monitoring in anisotropic shales. We consider a simple homogeneous anisotropic velocity model, with VTI (Vertical Transverse Isotropy) symmetry, as is commonly found in shales. We use a ray-based forward modeling approach to generate synthetic DAS data from the model, to investigate features of the data, further illustrated with examples from a real dataset. We demonstrate how simple patterns may be extracted from the data to quickly provide insight into useful parameters such as event distance, depth and fault-plane orientation. We envisage these techniques could be employed to rapidly analyze large datasets through more advanced algorithm development.

[Figure 1 about here.]

DATASET

We design our model based on a real microseismic dataset recorded during a single stage of a hydraulic fracturing stimulation. The data were aquired using a Silixa iDAS system recording strain-rate along a fiber optic cable deployed in a horizontal monitoring well. The stimulation occurred in a parallel well at the same depth located approximately 200 m away. The data were recorded at 2000 Hz along a standard fiber with 3765 channels with a 1 m channel spacing and a gauge length of 10 m.

Figure 1 shows the monitoring setup with event locations estimated from a surface geophone array. We note that most of the events occur near the depth of injection, with some events extending above, thus we expect most of the recorded ray paths to be nearly horizontal, but with some steeper arrivals, and all within a few hundred meters of the monitoring well.

Vertical and horizontal seismic velocities within the reservoir were estimated using cross-dipole sonic logs from the horizontal monitoring well, and a nearby vertical well. They were found to be strongly anisotropic. Assuming a VTI model, the anisotropy can be characterized using the vertical P- and S-wave velocities $V_{P0} = 2800$ m/s and $V_{S0} = 1750$ m/s; and the Thomsen (1986) parameters $\varepsilon = 0.42$, and $\gamma = 0.36$, which determine the horizontal velocities of P and SH, respectively. Thomsen's δ parameter controlling the P and SV velocities at intermediate inclinations could not be constrained by the vertical and horizontal sonic logs. However, for modeling purposes we have assumed that it is equal to half the ε (i.e. $\delta = 0.21$), which is a reasonable assumption for shales (Horne, 2013).

Figure 1b shows a plot of the predicted group velocity surfaces from the inferred velocity model. We note that P and SH waves are much faster in the horizontal direction than in the

vertical direction, and that for horizontal propagation there is a significant amount of shear-wave splitting (i.e. SH and SV have different wave speeds). For steeper inclinations, the gap between SH and SV wave narrows until they reach a singularity (the velocity surfaces cross) for inclinations of approximately 40° from vertical. For inclinations steeper than this singularity, SV is slightly faster than SH until they converge again along the vertical symmetry axis.

SYNTHETIC MODELING

Theory

We use a ray based approach to compute synthetic DAS data for a homogeneous VTI medium. Assuming a moment tensor point source, a ray-tracer is used to calculate travel-times to each channel for P, SV, and SH wave arrivals. Displacement amplitudes and polarizations are provided by dynamic ray theory Green's function derived by Chapman (2004,Chapter 5).

For a fiber oriented along the x axis we can relate the x-component of displacement (u_x) provided by the ray-tracer to strain along the fiber (e_{xx}) using the following relation (e.g. Daley et al., 2016):

$$e_{xx} = \frac{\partial u_x}{\partial x} = \frac{\partial u_x}{\partial t}\frac{\partial t}{\partial x} = \frac{\partial u_x}{\partial t} p_x, \tag{1}$$

where p_x is the x-component of the slowness of the phase in question. We see from this relation that there are two possible approaches to generating synthetic strain data. The first is to generate synthetic displacement data, project the displacement onto the cable axis direction, and simply compute the spatial derivative of the resulting waveforms along the fiber to find strain. The second option is to multiply the time-derivative of displacement

by the axial slowness. Since the slowness vectors are already computed as part of the ray tracing, we choose the second method.

To create the waveforms from the Green's function, we convolve them with a third-order Brune pulse source wavelet (Beresnev and Atkinson, 1997; Leaney, 2014):

$$s(t) = \frac{\omega_c^3 t^2}{2} e^{-\omega_c t} H(t), \tag{2}$$

where $\omega_c = 2\pi f_c$ with f_c being the corner frequency of the source spectra and $H(t)$ the Heaviside step function. Practically speaking, the time derivative in equation 1 can be applied to the source wavelet prior to convolution. Additionally, since the iDAS system records strain-rate ($\dot{e}_{xx}$) rather than strain, an additional time derivative is required.

At this point we have created synthetics of point measurements of infinitesimal axial strain-rate at each channel location. However, DAS systems do not record a point measurement, rather they measure the strain over a finite length along the fiber, known as the gauge length, centred at each channel. This acts as a spatial averaging filter along the cable equivalent to convolving with a boxcar function (Dean et al., 2017). Thus the DAS response at channel coordinate x_{ch} is approximately equivalent to

$$d_{DAS}(x_{ch}) = \frac{1}{L_G} \int_{x_{ch}-L_G/2}^{x_{ch}+L_G/2} \dot{e}_{xx} dx, \tag{3}$$

where L_G denotes the gauge length (Hartog, 2017).

Comparison with geophones

In this section, rather than model the DAS synthetics directly, we first model the more conventional geophone response showing particle velocity and then show the equivalent DAS response to highlight the difference (see Martin, 2018, for a discussion of this relationship

for isotropic media). For modeling purposes we consider Cartesian coordinate system with receivers (fiber optic cable) aligned along the horizontal x_1 axis, and a microseismic source located in the plane perpendicular to the midpoint of the array, offset in the horizontal (x_2) and vertical (x_3) directions.

[Figure 2 about here.]

The single-component nature of the recordings has some implications for the sensitivity of different body-wave phases depending on their propagation direction and polarization. In VTI media the P, SV and SH phases travel independently; P and SV waves are both polarized in the vertical plane containing the ray vector, with P polarized nearly parallel to the ray and SV nearly perpendicular, whereas SH waves are polarized in the horizontal axis perpendicular to this plane. In Figure 2a we consider a horizontal fiber and a microseismic point source offset from the fiber both horizontally and vertically. At the closest point to the array from the source, the first arrivals are purely broadside (i.e. the rays are perpendicular to the fiber); thus we expect high sensitivity to SH phases because they are polarized parallel to the fiber, but low sensitivity to P and SV because they are both polarized perpendicular to the fiber. Conversely, at long offsets along the cable the angle between the ray propagation direction and the fiber is small, such that there is a larger sensitivity to P and SV waves and smaller sensitivity to SH. For the special case of an event at the same depth as the cable, such that all rays are purely horizontal (Figure 2b), SV polarization is strictly vertical for all ray azimuths and is thus not recorded.

[Figure 3 about here.]

Figure 3a shows modeled particle velocity from a moment-tensor point-source recorded

along a horizontal array of receivers with 1 m spacing (equal to the channel spacing). It shows only the component of velocity projected on to the direction of the array. The source is located at a horizontal distance of 75 m from the array with a vertical offset of 30 m. As expected P and SV amplitudes both vanish at the apices of the moveout curves, where their polarizations are perpendicular to the arrays. Conversely, SH, which is polarized parallel to the fiber, shows peak amplitude at the apex.

To convert the particle motion to DAS strain-rate equivalent we take the spatial gradient of the particle velocity projected along the direction of the array (equation 1), and then apply a smoothing operator to account for the gauge length of 10 m (equation 3). An interesting, and somewhat counterintuitive consequence of this is that the peak SH amplitude in the particle velocities translates to zero amplitude when converted to DAS strain-rate (Fig 3b-c).

[Figure 4 about here.]

Figure 4 shows the resulting synthetic DAS data compared to an example of an observed microseismic event. In addition to the raw waveforms we have also plotted absolute amplitudes summed over space, which is useful for identifying the arrival time of the P and SH waves at the apex. Below the waveforms is a similar amplitude stack, but summed over time, which shows a very interesting pattern. Like the velocity data the strongest signal is contained in the SH phase; however, it is no longer centered at zero offset. Instead, there is a bimodal amplitude pattern with a local minimum at the zero-offset point to the fiber. This pattern closely matches those observed in real data.

Strain receiver sensitivity patterns

[Figure 5 about here.]

The contrast in the unimodal amplitude peak in SH observed in particle velocity versus the bimodal peaks in strain-rate highlights an important difference between geophones and DAS. Single-component geophone recordings involve the projection of a simple vector (particle displacement or velocity) onto the component axis, whereas DAS sensors involve projecting a tensor (strain or strain-rate) onto the cable direction, which inevitably results in more complex patterns. The strain sensitivity pattern of body waves depend on the relative orientation of their slowness and polarization vectors. Figure 5 shows DAS strain sensitivity patterns for P and SH waves propagating in the horizontal plane. For P waves (Figure 5a) the slowness and polarization vectors are parallel, which results in a $\cos^2\theta$ sensitivity pattern, where θ is the angle between the propagation vector and the fiber, resulting in maximum axial strain parallel to the propagation direction and zero strain perpendicular to it (e.g. Benioff, 1935; Kuvshinov, 2016). Conversely, for SH waves, the polarization and slowness vectors are perpendicular, such that the principal axial strain components are at 45° to both vectors and alternate in sign, varying like $\sin 2\theta$. This means that the DAS response to SH waves vanishes when measuring either perpendicular or parallel to the ray direction and will alternate between extension and compression for other angles. Note that these simple $\cos^2\theta$ and $\sin 2\theta$ relationships are only strictly true for isotropic media, or for propagation within the horizontal symmetry plane for VTI media. For inclined propagation of P and SV waves where phase and polarization vectors are not parallel or perpendicular the resulting sensitivity will be more complicated (e.g. Leaney et al., 2019).

Beyond these geometric effects on sensitivity of DAS to P and S waves, there is also a

wavenumber response due to the gauge length of DAS system (Martin, 2018; Karrenbach et al., 2019). This introduces notches in the sensitivity which depend on frequency, velocity and propagation direction relative to the fiber. See Karrenbach et al. (2019) for a more thorough discussion of this effect.

[Figure 6 about here.]

Given that the sensitivity is a geometric effect it is likely that we can use the separation distance between the bimodal amplitude peaks in SH observed in the data (Figure 4) to estimate the distance to the event from the array. Figure 6a shows axial strain along the fiber for SH arrivals modeled using ray theory for events located in the horizontal plane at 50 m, 200 m and 500 m from the cable. A uniform radiation pattern is used, and the modeled amplitudes include geometrical spreading. It is clear that the separation between the amplitude peaks is proportional to the distance of the event from the cable. We can estimate the distance to the event, d, by

$$d \sim \sqrt{2} x_{1/2}, \tag{4}$$

where $x_{1/2}$ is the half-width of the peak-to-peak distance. Figure 6b shows a similar plot, but for SV arrivals using events located in the vertical plane. Note that this also shows a bimodal pattern, but with much sharper and focused amplitude peaks. This is because of a ray-focusing effect for SV propagation at inclinations of ~40° due to the anisotropy. This effect is common for anisotropic shales where Thomsen's δ is less than ε. While the precise pattern is dependent on the Thomsen parameters, the angle inclination where it occurs is typically similar for most models. In some cases where $\delta \ll \varepsilon$ the ray focussing is large enough to cause the SV wavefront to fold in on itself causing shear-wave triplications or cusps (e.g. Thomsen and Dellinger, 2003; Baird et al., 2017).

In practice, the relationship between the observed amplitude patterns and distance may be more complex due to non-uniform source radiation patterns as well as arrivals from inclinations outside the anisotropic symmetry planes. Nevertheless, the separation of amplitude peaks provides a first-order estimate of event distance.

Event depth constraints

One of the major limitations of DAS recordings for microseismic monitoring is that the 1D nature of the recording makes it difficult to infer the directionality of waves and thus fully constrain the event locations. Some approaches to reducing the ambiguity include recording DAS in multiple wells simultaneously, or recording in both the horizontal and vertical sections of the same deviated well (e.g. Williams et al., 2017; Verdon et al., 2020). In the absence of more complex array geometries, however, insight into the directionality of waves may still be inferred by taking advantage of the anisotropy of the medium.

[Figure 7 about here.]

Here we demonstrate how the angular dependence of seismic velocities due to anisotropy can be used to constrain the inclination of the incoming waves, which when combined with estimates of event distance can be used to infer source location including event depth relative to the cable. To do this we model five microseismic sources, all located 100 m from the cable but at inclinations ranging from 90° (horizontal) to 0° (vertical) at 22.5° increments (Figure 7a). For the event located within the horizontal plane (Figure 7b), we might expect to observe significant shear-wave splitting based on the model's Thomsen parameters (Figure 1b). However, since all the ray-paths from the source to the fiber are horizontal, the SV phase is polarized in the vertical direction (Figure 2b), and does not

generate any axial strain along the horizontal cable, and thus is not observed in the DAS data.

The next source is placed at the same distance from the cable, but at a shallower source depth such that the incoming ray inclination at zero offset is steepened by 22.5° (Figure 7c). In this configuration the SV arrivals project a small horizontal component and generate axial strain along the fiber and hence it is observed on the DAS recording. At this inclination SH is still much faster than SV (Figure 1b) thus a significant amount of shear-wave splitting can be observed close to the apex and at longer offsets along the cable. This contrasts with the next source where the rays at the apex propagate at an inclination of 45° from vertical (Figure 7d), which is close to the inclination of the expected shear-wave singularity where the two shear waves propagate with the same velocity (Figure 1b). Thus, no S wave splitting is observed at short offsets along the cable, although it is observed at larger offsets since inclination shallows as you move along the cable, resulting in an increase in apparent shear wave splitting with distance.

At steeper inclinations SV is slightly faster than SH. The difference is not large enough to readily detect S-wave splitting close to the apex; however, we can see that the S-wave singularities are now offset from the apex (Figure 7e). Finally for events located vertically above (or below) the cable, only SV is recorded since SH is polarized perpendicular to the fiber (Figure 7f). We note that the moveout of SV is more complicated than that of SH, with an abrupt change in apparent slowness at ~80 m offset. This change is related to the ray focusing effect of the anisotropy, which also causes the sharp bi-modal amplitude peaks in the SV sensitivity pattern (Figure 6b), and thus provides a strong geometric indicator of event location. The precise inclination at which the ray focussing occurs depends on knowledge of the Thomsen parameters, including the δ parameter which can be difficult

to measure from sonic logs. However, the inclination typically falls within the relatively small range of 40-45° from vertical for a wide variety of shale anisotropies (Thomsen and Dellinger, 2003); thus it can provide good geometric constraints, even for cases where δ is not well known.

[Figure 8 about here.]

Figure 8 shows an observed microseismic event with weak P arrival followed by two larger amplitude S arrivals exhibiting clear S-wave singularities offset from the apex, compared with a synthetic event exhibiting similar features. The precise inclination of the singularities is dependent on the relative magnitudes of the Thomsen parameters. Nonetheless, if such singularities are observed it is a strong indicator of a steep incidence angle, and a good geometric constraint on the event location. Note also that the sharp amplitude peaks observed in the amplitude stack over time is similar to the sensitivity pattern expected for SV arrivals (Figure 6b), providing an additional indicator of steep arrival angle.

Source mechanism effects

To this point we have discussed how DAS recordings of microseimic data are dependent on the wave type, propagation angle relative to the cable axis and inclination in a VTI medium. Another important consideration, however, is the radiation pattern of the microseismic source. Figure 9 shows strike-slip radiation patterns in displacement (Figure 9a,d) and the e_{11} component of strain (Figure 9b,e) for P and SH waves in the horizontal plane. Figure 9c,f shows strain radiation for a rotated source mechanism such that the source symmetries and receiver symmetries are not aligned.

[Figure 9 about here.]

For P waves we see that the relationship between displacement radiation and strain radiation is quite simple. The fault plane and auxiliary plane separate the focal sphere into quadrants of outward- and inward-pointing displacement that coincide with quadrants of compressional and extensional strain in e_{11}, respectively. The additional effect of the receiver sensitivity (Figure 5a) acts to gradually fade out the broadside sensitivity of strain without introducing a polarity reversal.

Conversely, the SH radiation pattern is more complicated. We see that there are two sets of polarity reversals observed in the strain radiation. The first set is controlled by the source parameters defined by the planes bisecting the fault and auxiliary planes, which separate quadrants of displacement with a clockwise sense of rotation relative to the source from those with an anti-clockwise sense. This pattern will vary for different source mechanisms. The second pattern is controlled by the receiver geometry and is defined by the receiver sensitivity pattern (Figure 5b). This pattern remains fixed for all events and imposes polarity reversals for rays propagating parallel and perpendicular to the fiber.

[Figure 10 about here.]

Figure 10 shows synthetic DAS recordings of events with the mechanisms shown in Figure 9, located at the same depth as the fiber. The conventional approach to constrain fault plane solutions using geophones involves mapping the polarity of P waves to identify the nodal planes where the amplitude reduces to zero and their polarity reverses. However, given the low sensitivity for broadside P arrivals these polarity reversals can be hard to identify in DAS data when they occur at near offset. Conversely, SH polarity reversals can

be more readily identified due to the high amplitude of the SH recorded signal as well as the large aperture of the continuous fiber recording. It is impossible to fully constrain the moment tensor due to the 1D nature of the DAS recording, however if a double couple mechanism is assumed there are clear geometric relationships between the location of the polarity reversals observed in the SH and P phases and the orientation of the fault and auxiliary planes. Indeed recent studies have shown remarkable consistencies in the patterns of polarity reversals observed in DAS recordings of stimulated events (Cole et al., 2018; Karrenbach and Cole, 2019), suggesting this approach can be used to quickly constrain possible source mechanisms.

[Figure 11 about here.]

Figure 11a shows an observed microseismic recording with clear P, SH, and SV arrivals. We note that the highest amplitudes are observed in the SH arrival with a relatively weak SV arriving later. There is significant shear-wave splitting for all offsets along the cable indicating the incoming inclination is relatively shallow, though not horizontal. In addition to the polarity reversal in the apex of the SH arrival due to the receiver sensitivity pattern, we can also see clear polarity reversals due to the source radiation pattern at offsets of approximately −100 m and 190 m. These reversals can also be seen as local minima in the sum of absolute amplitudes over time plotted below, although it is not as clear as in the synthetics (Figure 10) due to the additional background noise.

In Figure 11b we attempt to reproduce many of the characteristics found in the observed event with a simple synthetic model. We place the source a horizontal distance of 100 m with a vertical offset of 65 m giving a zero-offset inclination of ~57° from vertical. Unique fault plane solutions are only possible if the three-dimensional pattern of amplitudes are

adequately sampled, which cannot be done with a simple 1D DAS recording. Instead, we choose a source mechanism based on a representative fault plane solution inferred from surface geophones, but with 10° anti-clockwise rotation in strike to better match the observed polarity reversals. Projections of the modeled polarity reversal locations along the cable have been overlaid on the amplitude stack of both the modeled and real data. We also show the confidence limits of these projections for fault strikes of $\pm 3°$. Thus, we have demonstrated that DAS recordings can be used to provide clear constraints and improvements to source mechanism estimates.

CONCLUSIONS

Using a ray-based method of creating synthetic waveforms we have explored some fundamental characteristics of microseismic data recorded on horizontal DAS arrays in VTI media, which may aid in constraining event locations and source mechanisms while reducing ambiguity in the directionality of waves. For events located close to the array depth, we have shown that the SH phase usually dominates the signal due to its polarization along the cable at near offsets. The amplitude of the SH phase along the cable produces a characteristic pattern with bimodal peaks surrounding the zero-offset point, with the separation between the peaks providing an indication of the distance of the event from the cable. A similar bimodal pattern can be observed in the amplitude of the SV phase for steep arrivals, but with much sharper amplitude peaks due to a ray focussing effect for SV common in anisotropic shales.

Insight into the event depth relative to the cable can be gained by observing characteristics of the shear-wave splitting. For events located in the horizontal plane, the SV phase will not be recorded because of its polarization perpendicular to the fiber. For events

above or below the horizontal plane the SV phase can be observed and the details of shear-wave splitting and how it changes with offset along the cable can provide insight into the near offset inclination. The presence of S-wave singularities, for example, provides a strong indication of a steep arrival. Using these features in VTI media can reduce some of the uncertainty of the directionality of waves inherent in using single-component data.

Finally, the effect of microseismic source mechanisms on the observed strain amplitude patterns was explored. Although moment tensors cannot be fully constrained using a single one-dimensional array, the high-fold continuous nature of DAS recordings allows for accurate picking of polarity reversals, particularly in the SH phase, providing strong constraints on possible fault plane solutions and allowing existing source mechanism estimates to be validated and calibrated.

As DAS arrays become increasingly used for microseismic monitoring in industrial settings, one of the major challenges is developing techniques to deal with the large data volumes associated with the dense spatial and temporal sampling provided by these systems. We have shown using synthetic modeling how simple patterns extracted from the data can be used to quickly provide estimates and constraints on event distance, inclination, and fault-plane solutions. Machine learning techniques provide a possible approach for rapidly classifying data using pattern recognition. Recent studies have shown great potential for event detection of DAS data using machine learning, and one could envisage expanding such systems to also classify events by distance, location and mechanism using simple pattern recognition.

ACKNOWLEDGMENTS

The authors thank Chevron ETC and Silixa Ltd. for permission to publish the work. We thank the reviewers and editors for their constructive comments, which helped improve the manuscript. This work was funded by the Natural Environment Research Council (NERC) under the FAST-MoDE project (Grant No. NE/R014531/1).

REFERENCES

Baird, A. F., J.-M. Kendall, Q. J. Fisher, and J. Budge, 2017, The role of texture, cracks and fractures in highly anisotropic shales: Journal of Geophysical Research: Solid Earth, **122**.

Benioff, H., 1935, A linear strain seismograph: Bulletin of the Seismological Society of America, **25**, 283–309.

Beresnev, I. A., and G. M. Atkinson, 1997, Modeling finite-fault radiation from the ω^n spectrum: Bulletin of the Seismological Society of America, **87**, 67–84.

Binder, G., and D. Chakraborty, 2019, Detecting microseismic events in downhole distributed acoustic sensing data using convolutional neural networks, *in* SEG Technical Program Expanded Abstracts 2019: Society of Exploration Geophysicists, 4864–4868.

Chapman, C., 2004, Fundamentals of seismic wave propagation: Cambridge University Press.

Cole, S., M. Karrenbach, D. Kahn, J. Rich, K. Silver, and D. Langton, 2018, Source parameter estimation from DAS microseismic data, *in* SEG Technical Program Expanded Abstracts 2018: Society of Exploration Geophysicists, 4928–4932.

Daley, T. M., D. E. Miller, K. Dodds, P. Cook, and B. M. Freifeld, 2016, Field testing of modular borehole monitoring with simultaneous distributed acoustic sensing and geophone vertical seismic profiles at Citronelle, Alabama: Geophysical Prospecting, **64**, 1318–1334.

Dean, T., T. Cuny, and A. H. Hartog, 2017, The effect of gauge length on axially incident p-waves measured using fibre optic distributed vibration sensing: Geophysical Prospecting, **65**, 184–193.

Hartog, A. H., 2017, An introduction to distributed optical fibre sensors: CRC press.

406 Horne, S., A. Baird, A. Stork, and G. Naldrett, 2019, Machine learning for DAS microseismic
407 event detection: Presented at the 81st EAGE Conference and Exhibition 2019 Workshop
408 Programme.
409 Horne, S. A., 2013, A statistical review of mudrock elastic anisotropy: Geophysical Prospect-
410 ing, **61**, 817–826.
411 Karrenbach, M., and S. Cole, 2019, DAS microseismic source mechanism estimation by
412 forward-modeling, *in* SEG Technical Program Expanded Abstracts 2019: Society of Ex-
413 ploration Geophysicists, 1004–1008.
414 Karrenbach, M., S. Cole, A. Ridge, K. Boone, D. Kahn, J. Rich, K. Silver, and D. Langton,
415 2019, Fiber-optic distributed acoustic sensing of microseismicity, strain and temperature
416 during hydraulic fracturing: Geophysics, **84**, no. 1, D11–D23.
417 Kuvshinov, B., 2016, Interaction of helically wound fibre-optic cables with plane seismic
418 waves: Geophysical Prospecting, **64**, 671–688.
419 Leaney, S., T. Mizuno, E. Velez, T. Cuny, and M. Perez, 2019, Integrated anisotropic model
420 building, DAS simulation and imaging, *in* SEG Technical Program Expanded Abstracts
421 2019: Society of Exploration Geophysicists, 999–1003.
422 Leaney, W. S., 2014, Microseismic source inversion in anisotropic media: PhD thesis, Uni-
423 versity of British Columbia.
424 Martin, E. R., 2018, Passive imaging and characterization of the subsurface with distributed
425 acoustic sensing: PhD thesis, Stanford University.
426 Parker, T., S. Shatalin, and M. Farhadiroushan, 2014, Distributed acoustic sensing–a new
427 tool for seismic applications: First Break, **32**, 61–69.
428 Thomsen, L., 1986, Weak elastic anisotropy: Geophysics, **51**, 1954–1966.
429 Thomsen, L., and J. Dellinger, 2003, On shear-wave triplication in transversely isotropic

media: Journal of Applied Geophysics, **54**, 289–296.

Verdon, J. P., S. A. Horne, A. Clarke, A. L. Stork, A. F. Baird, and J.-M. Kendall, 2020, Microseismic monitoring using a fibre-optic distributed acoustic sensor (DAS) array: Geophysics, **In press**, 1–48. DOI: 10.1190/geo2019-0752.1

Williams, A., J. M. Kendall, A. Clarke, and J. Verdon, 2017, Challenges in locating microseismic events using distributed acoustic sensors: Presented at the AGU Fall Meeting Abstracts.

LIST OF FIGURES

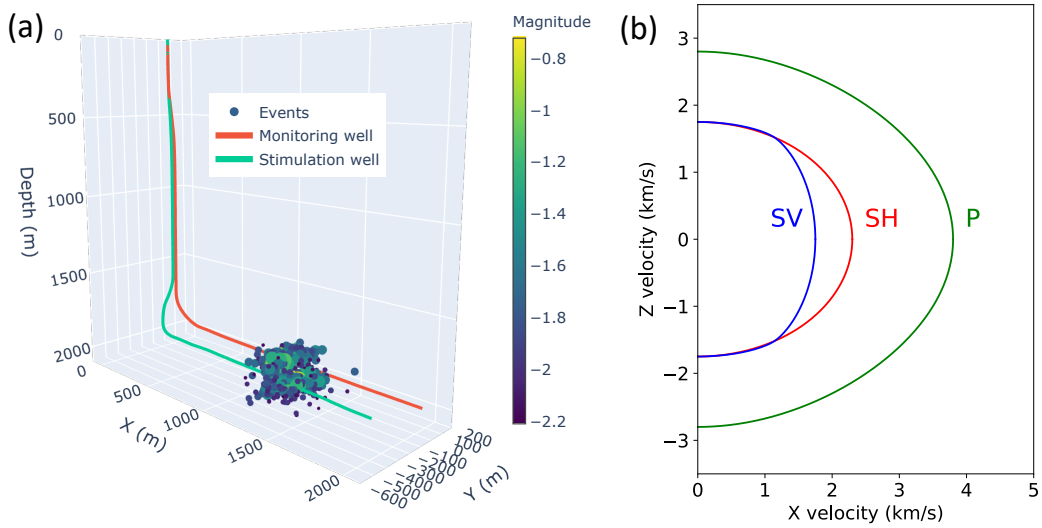

Figure 1: (a) Schematic diagram showing array geometry and event locations for the DAS dataset. (b) Group velocity surfaces for P, SV and SH waves for the homogeneous VTI velocity model based on cross-dipole sonic logs in the reservoir. Polar angle from the origin indicates ray propagation vector.

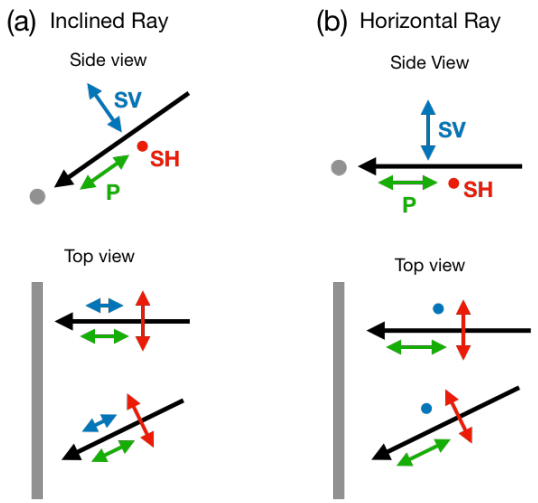

Figure 2: Cartoon showing polarization vectors for P (green), SV (blue) and SH (red) waves relative to horizontal array geometry for (a) and inclined ray, and (b) a horizontal ray. Sensitivity for geophones is controlled by the projection of the polarization vector on to the receiver component, thus we expect high sensitivity for broadside SH arrivals and low sensitivity for broadside P and SV arrivals.

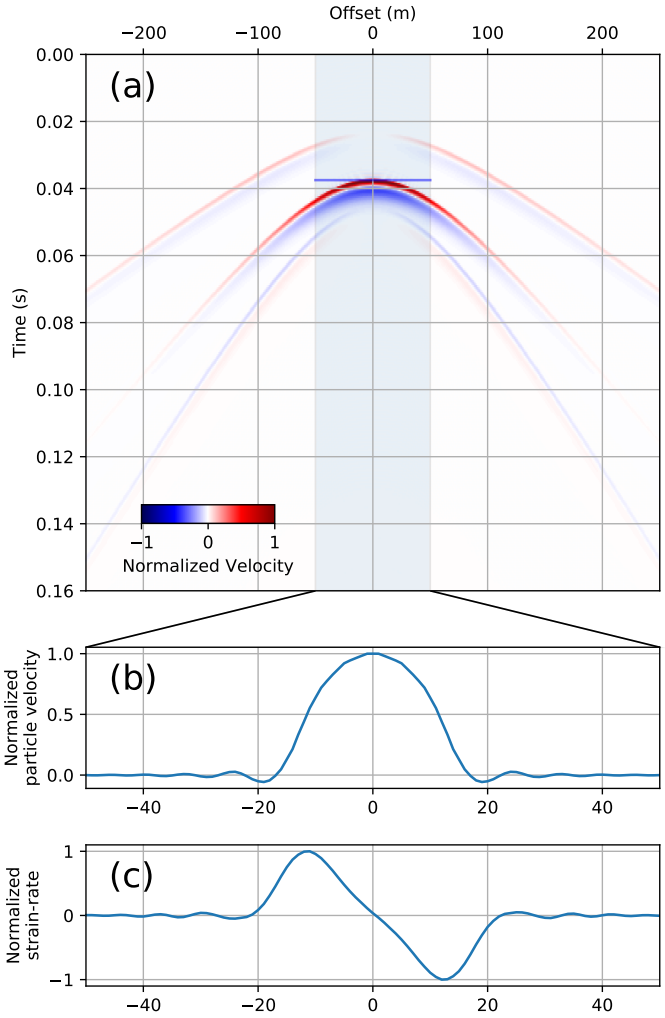

Figure 3: (a) Modeled particle velocity along the horizontal well direction for a microseismic source in a homogeneous VTI medium. The lower panel shows snapshots of (b) particle velocity and (c) strain rate along the fiber axis direction at the peak amplitude of SH arrival (indicated by blue horizontal line in (a)). Since strain rate is the spatial derivative of particle velocity along the fiber the peak amplitude for particle velocity translates to zero amplitude in DAS data.

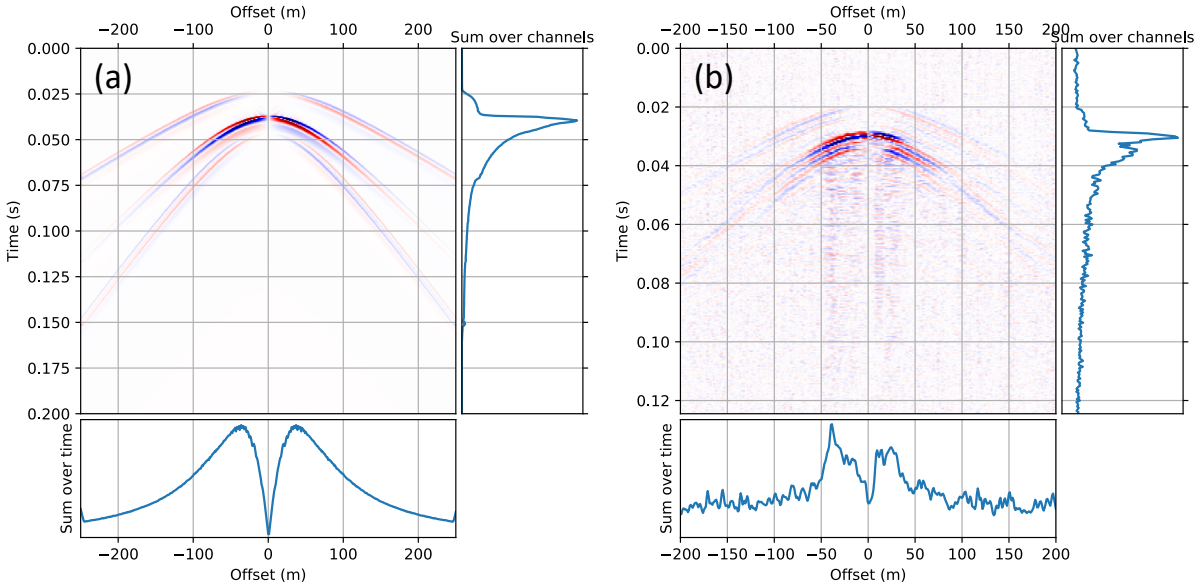

Figure 4: (a) Synthetic DAS data along a horizontal well for a microseismic source in a homogeneous VTI medium. (b) An example of observed microseismic event recorded on a DAS. To improve signal to noise in the observed data frequency-wavenumber (f-k) filtering has been applied to suppress frequencies above 300 Hz and wavenumbers above 0.1 m^{-1}. Plots to the right and below the waveforms show the absolute amplitudes summed over space and time, respectively.

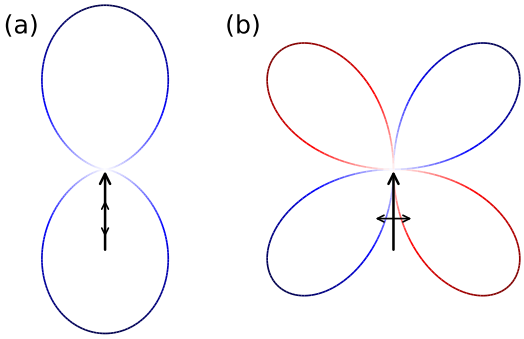

Figure 5: Top view of axial strain on a horizontal fiber as a function of fiber angle for (a) a horizontally propagating P wave and (b) a horizontally propagating SH wave. Polar angle indicates fiber orientation. Large arrow indicates ray propagation direction with smaller double-headed arrows indicating polarization direction. Blue lines indicate compression and red extension.

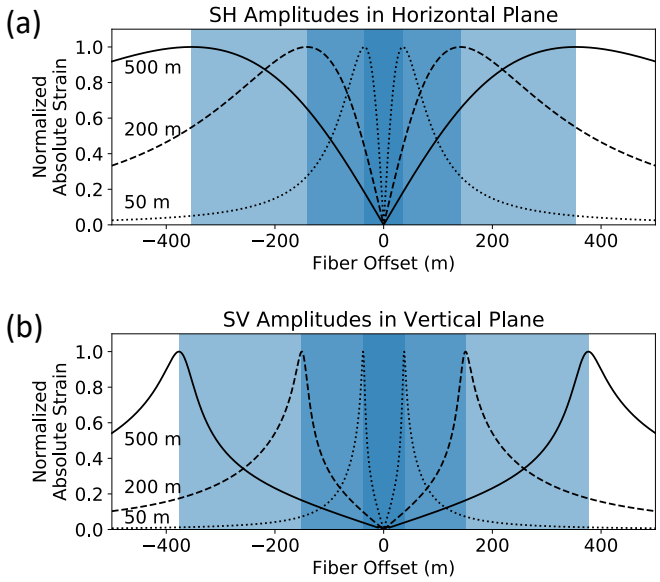

Figure 6: Predicted axial strain of the (a) SH and (b) SV, phases as a function of fiber offset for sources of uniform radiation pattern with varying distances from the fiber within the horizontal and vertical planes, respectively. The blue rectangles indicate the separation along the cable between the bimodal amplitude peaks, which is proportional to the distance to the source. Note that the sharp amplitude peaks in SV are due to the ray focussing effect of the VTI anisotropy.

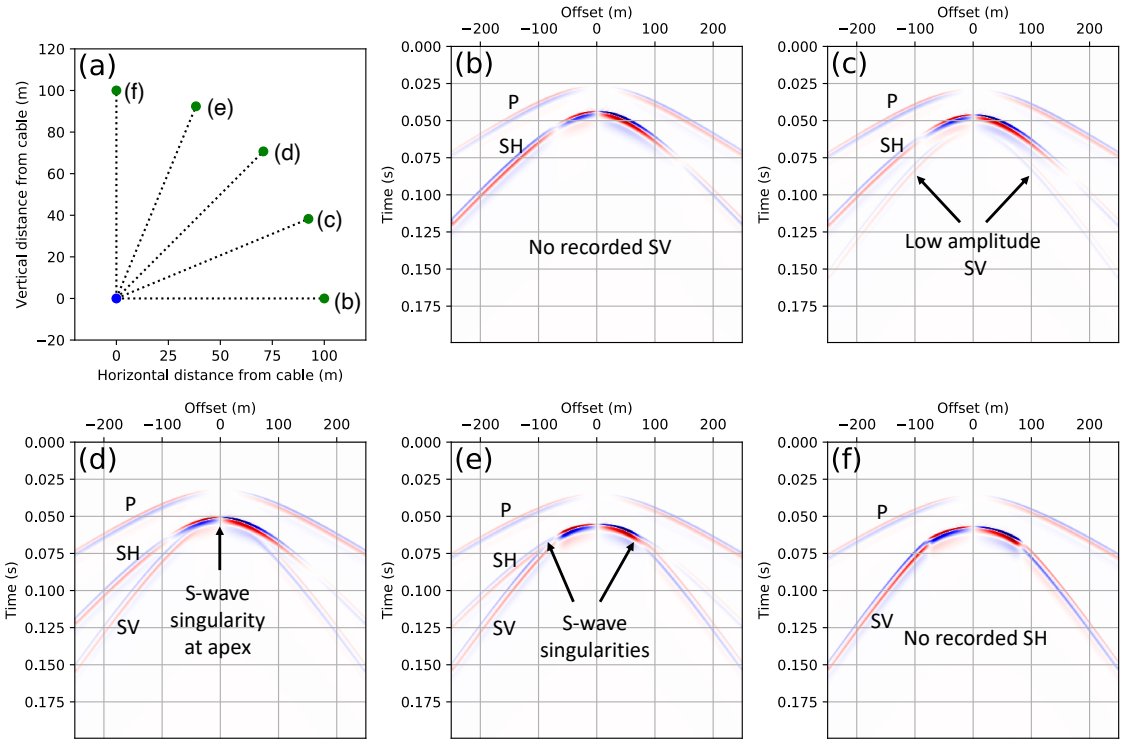

Figure 7: Synthetic DAS data for events located 100 m from the horizontal cable in a VTI medium at progressively steeper inclinations from horizontal. Panel a: Cross-section view showing the source locations (green dots, labelled b to f) distributed around the fiber (blue dot). Dashed lines indicate the ray paths at zero offset. Panels b-f: Synthetic DAS data for each event.

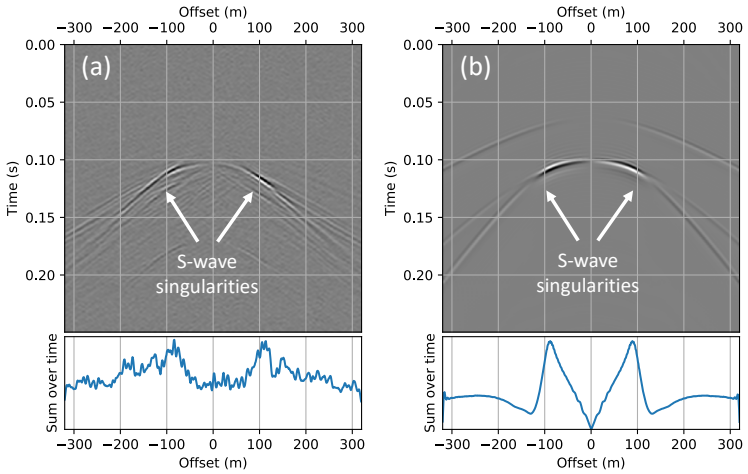

Figure 8: Observed DAS recording (a) of an event showing S wave singularities compared with a synthetic example (b) showing a similar feature. The synthetic event was modeled at a distance of 180 m from the cable with an incoming inclination of 25° from vertical. The presence of S wave singularities is a strong indicator of a steep incident angle. Note also the sharp amplitude peaks in SV similar to the sensitivity pattern expected for SV arrivals for steep propagation angles (Figure 6b). Real data in (a) has been filtered as described in Figure 4.

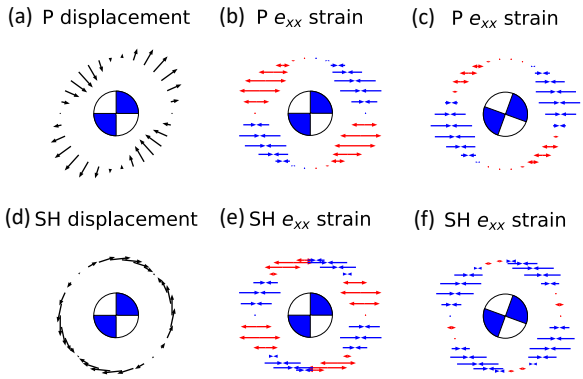

Figure 9: Radiation pattern for a strike-slip source mechanism in terms of (a) displacement and (b) the e_{11} component of strain for P waves. (c) Same as in (b) but with the source mechanism rotated such that the symmetries of source radiation and receiver sensitivity patterns are misaligned. (d-f) Same as (a-b) but for SH waves. Black arrows indicate particle displacement; colored arrows represent extensional (red) or compressional (blue) strain.

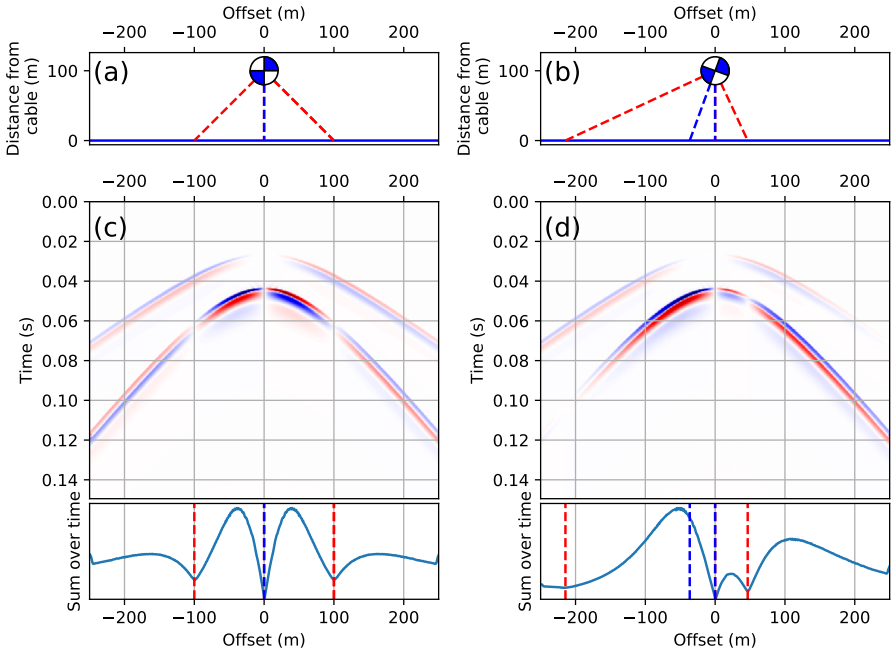

Figure 10: Example synthetic DAS recordings due to the source mechanisms shown in Figure 9b and c, with the event at the same depth as the fiber. Panels a and b show a map view of source location relative to cable (blue line). Panels c and d show the synthetic recordings along the cable, and a stack of absolute amplitudes summed over time. Dashed lines indicate projections of polarity reversals in: SH due to receiver sensitivity (black), SH due to source mechanism (red) and P due to source mechanism (blue).

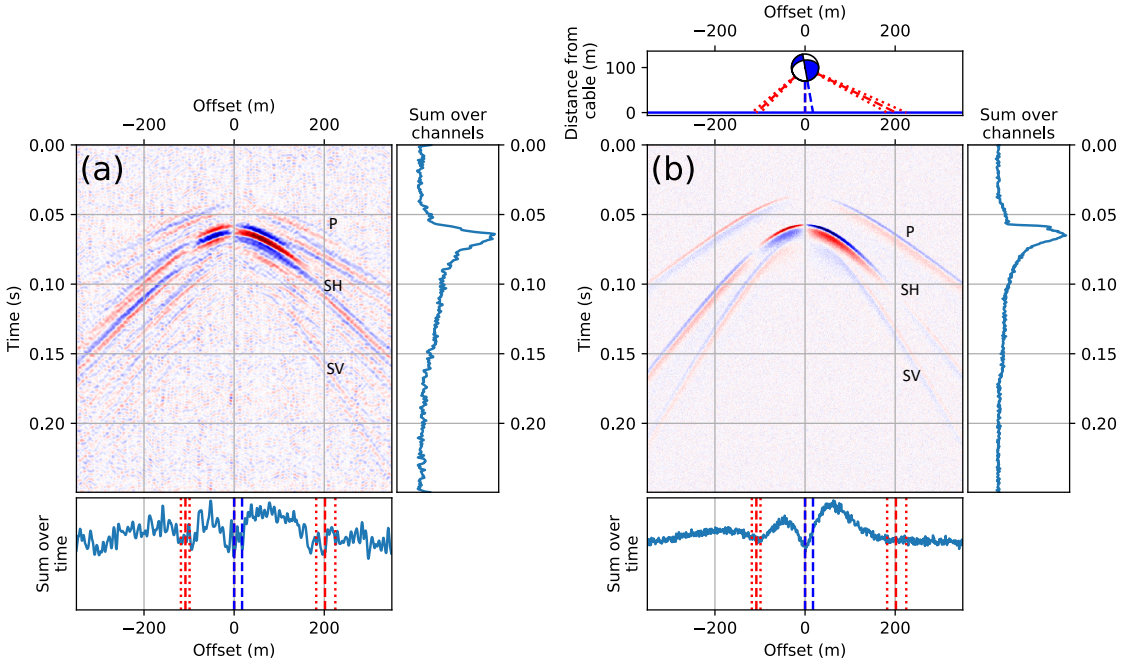

Figure 11: (a) Example DAS recording of an event with clear P, SH and SV arrivals, with polarity reversals observed in the SH and P. (b) synthetic event showing many of the same features as the observed recording. The modeled event is located at a horizontal distance 100 m and a vertical offset of 65 m above the cable. The source is modeled with a strike/dip/rake of 350°/90°/-120°, similar to mechanisms inferred from surface stations but with a slight rotation in strike to better match the observed polarity reversals. Red and blue dashed lines indicate projections of the modeled polarity reversals on the amplitude stack for SH and P waves, respectively. Dotted red lines indicate predicted SH polarity reversals if the fault strike were varied by ±3°. Real data in (a) has been filtered as described in Figure 4.